Graphene-like sulfur-doped g-C_3N_4 for photocatalytic reduction elimination of $UO_2{}^{2+}$ under visible Light

Lin Ke [a], Peifeng Li [a], Xi Wu [a], Shujuan Jiang [a,*], Mingbiao Luo [a], Yunhai Liu [a,*], Zhanggao Le [a], Chuanzhi Sun [b,*], Shaoqing Song [a,*]

[a] Key Laboratory for Radioactive Geology and Exploration Technology, Fundamental Science for National Defense, East China University of Technology, Nanchang 330013, PR China
[b] College of Chemistry, Chemical Engineering and Materials Science, Shandong Normal University, Jinan 250014, PR China

ARTICLE INFO

ABSTRACT

Owing to the unique electronic and optical properties, the graphene-like carbon nitride (C_3N_4) materials have attracted widespread interest. However, the exfoliation of bulk C_3N_4 into graphene-like structure is inhibited by the planar hydrogen bond between strands of polymeric melon units with NH/NH_2, due to the higher electronegativity of N with respect to C atoms. Herein, graphene-like sulfur-doped C_3N_4 (SC_3N_4) samples were successfully prepared by introducing sulfur into C_3N_4 to weaken the planar hydrogen bonding, and investigated as catalysts to photoreductively eliminate uranyl ion in aqueous media. Both experimental and computational perspectives confirmed that S-doping in SC_3N_4 can modify its electronic structure, reflected by the elevated conduction and valence band levels, as well as the improved transportation capability of photogenerated electrons. As a result, the photoactivity for $UO_2{}^{2+}$ photocatalytic reduction over the optimal SC_3N_4 was significantly improved, with apparent rate value reaching $0.16\,min^{-1}$ under visible-light irradiation, which was 2.28 times that over C_3N_4. This study provides an effective strategy for designing efficient visible-light-responsive photocatalysts for environmental remediation.

© 2016 Elsevier B.V. All rights reserved.

1. Introduction

Optimizing semiconductor materials to be efficient photocatalysts has attracted widespread concern due to its promising application in the energy production and environmental remediation [1–6]. Among numerous semiconductor photocatalysts, graphitic type carbon nitride (C_3N_4) is considered as a visible-light-driven material possessed the band-gap energy of ∼2.7 eV, suitable conduction and valence bands for hazardous contaminant elimination, water splitting, and carbon dioxide reduction [7–16]. As such, C_3N_4 has promptly become as a shining star material in the field of photocatalysis. Nevertheless, C_3N_4 always suffer from drawbacks, e.g., low photocatalytic efficiency due to the high excition dissociation energy, poor charge mobility, as well as lower specific surface area [17–20]. And some strategies (e.g., doping with heteroatoms, tuning morphology, loading plasmonic noble metals) have been used to solve these problems [21–35]. Actually, the C_3N_4 composed by tri-s-triazine rings could be supposed to possess graphite-type layer framework, and there are strong covalent C—N bonding among layers and poor van der Waals effect in layered structures [36,37]. enlightened by the transformation from graphite to graphene with the Hummers' strategy, it would be seemingly possible to prepare graphene-like C_3N_4 with monolayer or a few layers which would thus exhibits unique electronic and optical properties [38–42]. Recent experiments confirmed that Hummers method and thermal condensation can be used to synthesize C_3N_4 particles with thickness of several hundred nanometers, but not C_3N_4 with few layers. This is because a large amount of planar hydrogen bonding is formed among melon polymer linked to NH/NH_2 due to the larger electronegativity of N ($\chi(N) = 3.04$) with respect to C atoms ($\chi(C) = 2.55$). In principle, exfoliation of C_3N_4 to graphene-like C_3N_4 can be achieved by weakening the planar hydrogen bonding, therefore, the graphene-like C_3N_4 may be designed when an element (e.g., sulfur) with similar electronegativity to C is used to partially replace N of C_3N_4 through Hummers method or thermal oxidation exfoliation strategy. Thus, graphene-like C_3N_4 will supply good photocatalytic activity for heavy metal pollution elimination, water splitting, and carbon dioxide reduction conversion.

* Corresponding authors.
 E-mail addresses: sjjiang@ecit.edu.cn (S. Jiang), yhliu@ecit.edu.cn (Y. Liu), suncz@sdnu.edu.cn (C. Sun), sqsong@ecit.edu.cn (S. Song).

Uranium is the typical heavy metal pollutant that has caused severe environmental and public health problems primarily due to the chemical and radiological toxicity [43,44]. As a metal, uranium is not degradable, and thus strategies for its remediation mainly depend on decreasing its transport and bioavailability. Generally, adsorption methods shows highly efficient for removing uranium pollution, however, due to the limited saturation of the adsorption material and the surrounding environment variety, uranium pollutant is likely to be returned to the aqueous system, which will cause secondary pollution. We know that radioactive U exists in many chemical valence (such as U^0, U^{3+}, U^{4+}, and U^{6+}), and soluble U^{6+} and less soluble U^{4+} have been detected as the main species in the natural world [45–48]. Therefore, existence of U in the natural world is obviously influenced through the oxidation-reduction conversion between soluble U^{6+} and less soluble U^{4+}. In this paper, we aimed to use photoreductive technology to remove UO_2^{2+} from aqueous solution, and the graphene-like sulfur-doped C_3N_4 (SC_3N_4) samples as the photocatalysts were successfully prepared by introducing S into C_3N_4 to weaken the planar hydrogen bonding for photoreductive elimination of UO_2^{2+}. And the SC_3N_4 with the desirable electronic structures and graphene-like morphology were probed with spectroscopy analysis. The improved electronic structures of the SC_3N_4 exhibited potentiality for enhancing photoreduction reactivity in the elimination reaction of UO_2^{2+} pollutant. The essence including graphene-like framework, S chemical states and locations, and the corresponding photoreductive activity was explored both experimentally and theoretically for further designing potentially efficient UO_2^{2+} photoreduction materials.

2. Experimental section

2.1. Photocatalysts preparation

The SC_3N_4 samples were prepared by heating a mixture of urea (10 g) and benzyl disulfide (1 g) under the Ar atmosphere. In detail, urea and benzyl disulfide were first ultrasonically dissolved in ethanol for 25 min and then agitated for 1 h. Afterwards, the resulting mixture was dehydrated in a vacuum at 60 °C for 2 h, and subsequently placed in the quartz tube of a horizontal furnace. The temperature was ramped at 3.5 °C min^{-1} up to 560, 600 or 650 °C in Ar flow and maintained for 2 h. After that, the reactor was spontaneously cooled down to room temperature under Ar atmosphere. The resulting product was referred to as SC_3N_4-1, SC_3N_4-2, and SC_3N_4-3, corresponding to the annealing temperature at 560, 600, 650 °C. For comparison, a g-C_3N_4 sample was synthesized by directly heating 10 g of urea in a horizontal furnace at 560 °C.

2.2. Characterization

Micrographs were characterized with transmission electron microscopy (TEM, JEM-2100F). Brunauer-Emmett-Teller (BET) area value was detected with ASAP2020 N_2 adsorption instrument, and degassing was performed at 180 °C before detection. Crystal structure was characterized using X-ray diffraction XRD, Rigaku RINT-2000 instrument equipped with Cu Kα. The surface chemical component and oxidation states of photocatalysts were investigated with X-ray photoelectron spectroscopy (XPS). The binding energies of XPS spectrum were referenced C 1s at 284.6 eV. UV–vis diffuse reflection spectrum was obtained by UV–vis spectrophotometer (UV-2550, Shimadzu, Japan). Time-resolved fluorescence emission spectrum was conducted at Ambient temperature (Edinburgh Instruments, FLSP-920). Samples on glass cover slip were excited by an oil objective system with a circular-polarized 405 nm pulsed laser. In the test process, we ensured the emission can passed a slit equipment and enter imaging spectrograph system.

2.3. Photocatalysis tests

The photocatalytic reduction elimination of UO_2^{2+} was conducted at approximate 25 °C in a gas-protected system. In the photocatalytic reduction process, 0.10 g SC_3N_4 was placed into 200 mL of 0.12 mM UO_2^{2+} solution containing 5 mL of methanol. $(UO_2)_3(OH)^{5+}$ and $(UO_2)_4(OH)^{7+}$ were the major valence components at pH = 7 in accordance with visual MINTEQA calculation [49,50], and the surfaces of g-C_3N_4 and SC_3N_4 samples were negatively charged as measured by the Zeta potential tests (Fig. S1). Therefore, the photoreduction elimination was regulated at approximate pH = 7 by using sodium hydroxide aqueous solution. A 350 W Xe lamp ($\lambda \geq 420$ nm) was utilized to illuminate the photoreduction reaction. Prior to illumination, the photoreduction was eliminate O2 by argon bubbling for, and then this mixed solution was placed in the dark with magnetic stirring for 2 h to achieve adsorption balance. In the illumination process, about 4 mL of suspension was taken from the reactor system at a scheduled interval and centrifuged. The UO_2^{2+} content in the supernatant solution was detected with UVmini-1240 by Arsenazo III Spectrophotometric technology at 650 nm. This measured absorbance with illumination time was converted to photoreduction elilination efficiency of UO_2^{2+} in accordance with the equation:

Photoreduction efficiency of $UO_2^{2+} = (A_0 - A_t)/A_0 \times 100\%$, here A_0 and A_t are the absorbance intensities at time 0 (that is, after the absorption balance) and t min, respectively. After photoreduction reaction, photocatalyst was collected by centrifugation, and washed by the 1 mol/L HNO_3 to eliminate UO_2 on the SC_3N_4, and further washed with the deionized H_2O. Then, photocatalyst was dehydrated in vacuum at 60 °C for 2 h.

2.4. DFT calculations

DFT calculation was performed by the Gaussian 09 suite of computational programs. The computation was conducted at the PBE/6-31G*(C, H, N and S)/LanL2DZ(U) level to theoretically investigate electronic structures of C_3N_4 and SC_3N_4. The atomic structures of g-C_3N_4 and SC_3N_4 were constructed with a truncated structure composed by three melons, and three possibilities of N replaced by S were suggested. The fringe C/N atoms were compensated by H to eliminate boundary influence.

3. Results and discussion

3.1. Morphology and composition of SC_3N_4 samples

Morphology of C_3N_4 and SC_3N_4 samples were observed by TEM, as shown in Fig. 1. The pristine g-C_3N_4 sample displays porous layer structure with several nanosheets (Fig. 1A). In Fig. 1B–D, SC_3N_4 samples mainly show the graphene-like flake structure but without the pores as in g-C_3N_4, which are more transparent than the pristine g-C_3N_4. The obtained graphene-like structure is beneficial to the photocatalytic reaction, because the photogenerated electrons can conveniently transfer with absorbing the small amount of light energy [51]. Moreover, the BET specific surface areas of the g-C_3N_4 and SC_3N_4 samples were calculated to be 20.2, 120.7, 208.6, and 298.2 m^2/g for the g-C_3N_4, SC_3N_4-1, SC_3N_4-2, and SC_3N_4-3, respectively. The gradually increased surface area of g-C_3N_4, SC_3N_4-1, SC_3N_4-2 to SC_3N_4-3 will facilitate UO_2^{2+} adsorption.

Fig. 2 presents the XRD patterns of SC_3N4. The representative inter-layer stacking (002) peak could be examined at 27.4°, indicating the unique graphitic structure of g-C_3N_4; and the weak diffraction signal at 13.1° ascribed from (100) plane, which represents in-plane graphene structure [27,30,32,52]. Obviously, overall weakened intensity is confirmed for SC_3N_4 samples, indicating that
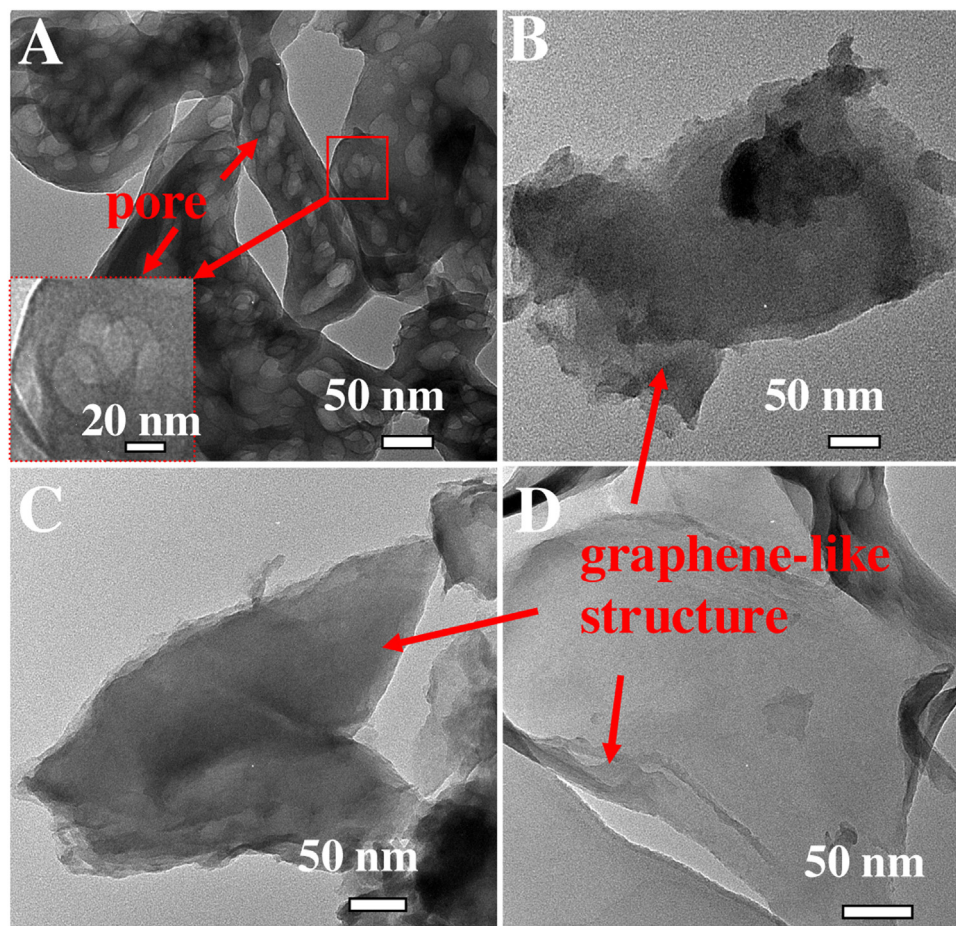
Fig. 1. TEM images for g-C$_3$N$_4$ (A), SC$_3$N$_4$-1 (B), SC$_3$N$_4$-2 (C) and SC$_3$N$_4$-3 (D).
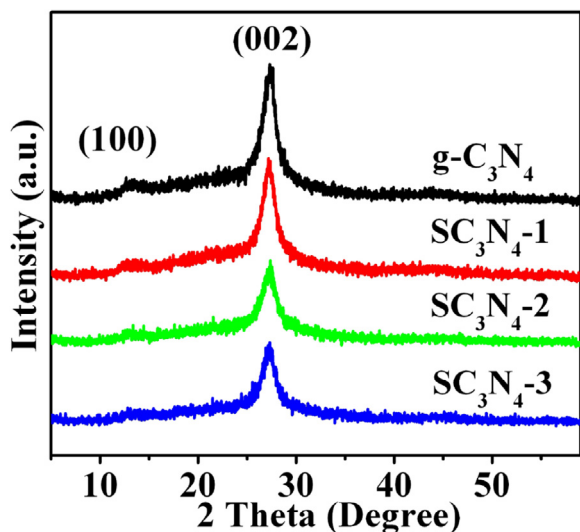

Fig. 2. XRD patterns of g-C$_3$N$_4$, SC$_3$N$_4$-1, SC$_3$N$_4$-2 and SC$_3$N$_4$-3.

lower characteristic diffraction signal strength by comparing with C$_3$N$_4$ due to the effect of formed graphene-like structure [39–41]. The surface species and chemical valences of the graphene-like SC$_3$N$_4$ were probed with XPS (Fig. 3). It can be seen that C 1s spectrum is composed by the standard reference C and the sp^2 bonded C in the N=C−N at 284.6 eV and 288.0 eV (Fig. 3A), respectively. Each N1 s spectrum can be ascribed to N characteristic of

C=N−C (398.8 eV), C$_3$−N (399.6 eV), and C−N−H (401.4 eV) [31]. The S 2p spectra were deconvoluted into two species, that is, the main signal at 163.9 eV arises from the C–S bonding in SC$_3$N$_4$ by replacing the latticed N with S, and the weak signal at 166.1 eV corresponded to C−SO$_x$−C bond [53]. Furthermore, the intensity of signal at 163.9 eV increased with increasing annealing temperature, coupled with a progressively increased C–S content from 0.11% to 0.37% and 0.47% corresponding to SC$_3$N$_4$-1, SC$_3$N$_4$-2, and SC$_3$N$_4$-3. Combined with the TEM charactrization results of the SC$_3$N$_4$ samples, it can be seen that the nanosheets of SC$_3$N$_4$ became thinner with the increased S content. The results indicate that transformation of C$_3$N$_4$ to graphene-like SC$_3$N$_4$ can be achieved by weakening the planar hydrogen bonding when S was introduced to partially replace N of C$_3$N$_4$. These successfully prepared graphene-like SC$_3$N$_4$ samples provide a suitable platform to investigate electronic structure and activity of SC$_3$N$_4$ for the photoreduction elimination of UO$_2^{2+}$.

3.2. Electronic structure of SC$_3$N$_4$

Electronic structures of C$_3$N$_4$ induced through doping S atom were revealed using UV–vis absorption spectroscopy. As seen in Fig. 4A, the absorption edges of the SC$_3$N$_4$ samples ranged from 500 to 530 nm compared with that of g-C$_3$N$_4$ at 458 nm, indicating an obvious red shift after the introduction of S into the lattice of g-C$_3$N$_4$. According to the Kubelka-Munk function vs. the energy of the absorbed light, the eigen band-gap energy decreased from 2.74 (C$_3$N$_4$) to 2.46 (SC$_3$N$_4$-1), 2.35 (SC$_3$N$_4$-2) and 2.10 eV (SC$_3$N$_4$-3) (Fig. 4B). According to intercept value of Fig. 4C, the conduction
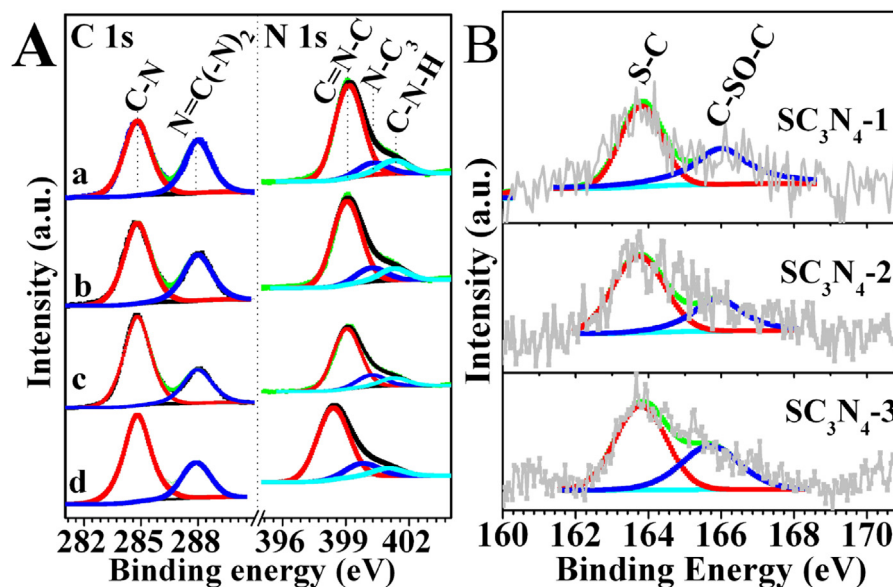
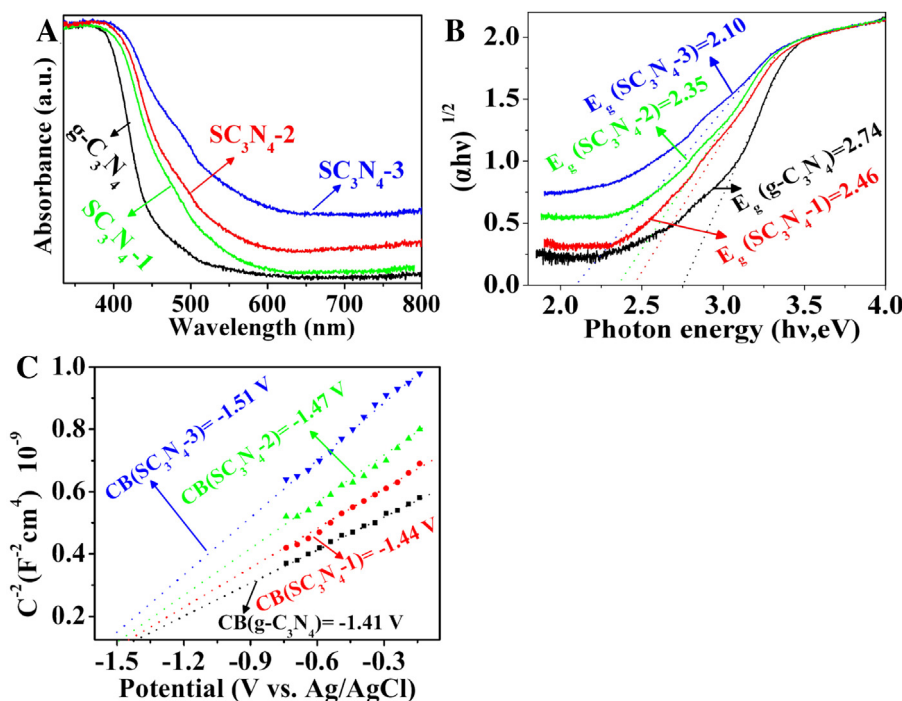**Fig. 3.** High-resolution XPS spectra of C1s, N 1 s (A) and S 2p (B) in SC_3N_4 samples.

Fig. 4. (A) Optical absorption spectra of g-C_3N_4 and SC_3N_4 samples; (B) Plots of $(\alpha h\upsilon)^{1/2}$ vs. photon energy (hυ) and (C) Electrochemical Mott-Schottky plots of g-C_3N_4 and SC_3N_4 samples.

band (CB) potential was approximate −1.41, −1.44, −1.47, and −1.51 V (vs. Ag/AgCl), that is, −1.18, −1.21, −1.24, and −1.28 V (vs. SHE) for C_3N_4, SC_3N_4-1, SC_3N_4-2, and SC_3N_4-3, respectively. The valence band (VB) potential of the samples was calculated to be 1.56 (g-C_3N_4), 1.25 (SC_3N_4-1), 1.11 (SC_3N_4-2) and 1.02 (SC_3N_4-3) V vs. SHE. Obviously, the electronic structures with the elevated CB and VB potentials has been constructed in SC_3N_4 samples. Combined with the TEM and XPS results, it is seen that the formation of graphene-like structure due to sulfur doping plays an important role for improving the electronic structure of SC_3N_4. However, the exact position of substitutional S cannot be identified experimentally, and hence we carried out DFT calculation to probe electronic structure of SC_3N_4.

Atomic structure model of C_3N_4 composing with melon units was constructed in Fig. 5A. Three types of periodic N atoms exist in the melon system, as marked with 1, 2, and 3. The Gibbs free energy of S for replacing N of the three sites was calculated to be −2344.50 (site 1 substitution), −2344.51 (site 2 substitution), and −2344.35 Hartree (site 3 substitution), indicating that site 2 is energetically favorable for substitutional doping. Moreover, the difference between the highest occupied molecular orbital and the lowest unoccupied molecular orbital was calculated to be 1.96 eV (C_3N_4), 0.26 (site 1 substitution), 0.43 (site 2 substitution) and 0.83 eV (site 3 substitution). It is worth noting that both HOMO and LUMO show upward shift for the case of site 2 substitution, which is different from those of site 1 and site 3 substitutions.
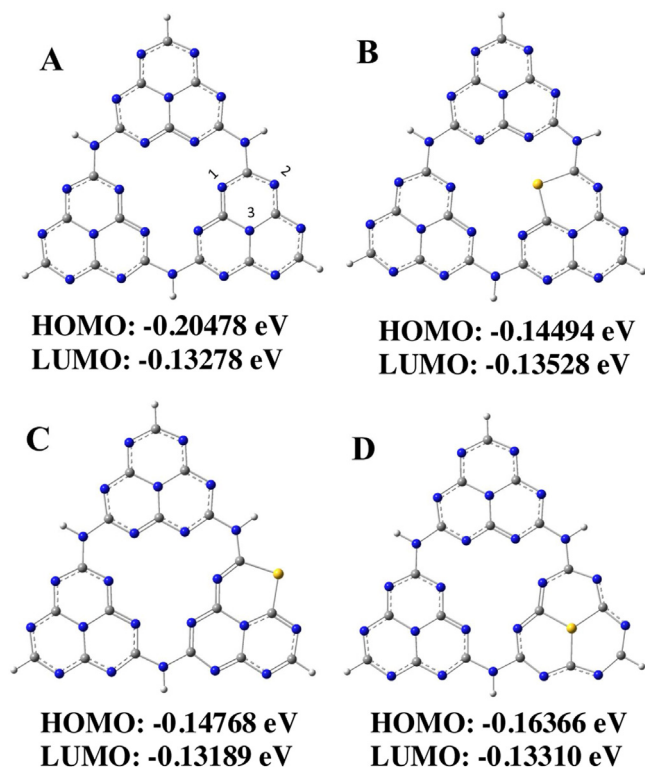
Fig. 5. (A) Molecular orbital energies and structures of the g-C$_3$N$_4$ (A) and SC$_3$N$_4$ with substitutional sulfur for nitrogen of site 1 (B), site 2 (C) and site 3 (D). Gray: C, blue: N and Yellow: S.

The substitutional S for N of site 2 to form graphene-like structure should be in best agreement with the experimental results among the three cases. The narrowed band gap with elevated CB and VB

levels indicates that the formed graphene-like structure by S doping supplies chance to enhance the activity of the C$_3$N$_4$ photocatalysts for photoreduction reaction.

3.3. Photoreduction performance

Photoactivities of SC$_3$N$_4$ and the pristine C$_3$N$_4$ were investigated in the photoreduction elimination of uranyl ions. As can be seen from Fig. 6A, uranyl ions solution without semiconductor was illuminated for 35 min, and content presents no noticeable decline, suggesting that uranyl is stable, and the self-photolysis for UO$_2^{2+}$ hardly occurs. In the presence of the photocatalysts, the UO$_2^{2+}$ ion concentration only slightly decreased during the 125-min adsorption experiments in the dark, and remained constant after the first 60 min, indicating the achievement of the adsorption balance between semiconductor and uranyl. Upon visible-light irradiation, reduction reaction of uranyl ions reacted obviously within 35 min using C$_3$N$_4$ and SC$_3$N$_4$ photocatalysts. In detail, the photocatalytic activity of g-C$_3$N$_4$ and SC$_3$N$_4$ samples was greatly different, e.g., after visible-light irradiation for 15 min, the elimination efficiency of UO$_2^{2+}$ over g-C$_3$N$_4$, SC$_3$N$_4$-1, SC$_3$N$_4$-2 and SC$_3$N$_4$-3 were 58%, 70%, 85% and 92%, respectively. The photocatalytic activity of the four samples followed the order: SC$_3$N$_4$-3 > SC$_3$N$_4$-2 > SC$_3$N$_4$-1 > g-C$_3$N$_4$, and the reaction rate (k) was 0.16, 0.12, 0.09 and 0.07 min^{-1} according to the pseudo-first-order equation (i.e., ln(C/C_0) = kt) [31,54,55], (Fig. 6B). Particularly, the k value of the SC$_3$N$_4$-3 sample was 0.16 min^{-1}, which was 2.28 times of g-C$_3$N$_4$ (0.07 min^{-1}), suggesting the improved activity of SC$_3$N$_4$ by sulfur doping. After the photocatalytic reduction of UO$_2^{2+}$, the uranium species on the surface of SC$_3$N$_4$ photocatalyst was revealed by XPS (Fig. S2 in Supplementary material), and the XPS spectrum confirmed that U(VI) and dominant U(IV) coexisted on the SC$_3$N$_4$, indicating that most of U(VI) was photocatalytically reduced to U(IV) over SC$_3$N$_4$ photocatalysts.
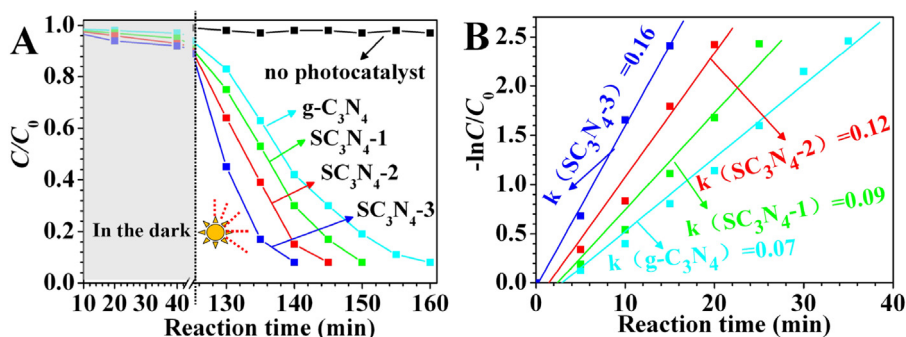

Fig. 6. (A) The variation of UO$_2^{2+}$ concentration vs. illumination time with g-C$_3$N$_4$ and SC$_3$N$_4$ as photocatalysts; and (B) pseudo-first-order rate constant (k) of UO$_2^{2+}$ reduction with g-C$_3$N$_4$ and SC$_3$N$_4$ as photocatalysts.
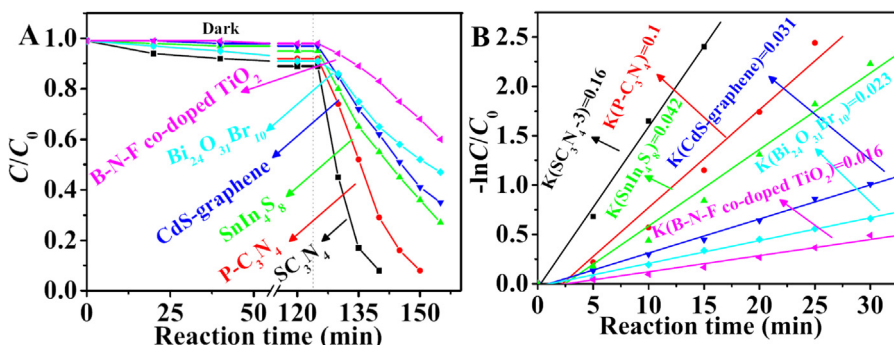

Fig. 7. The variation of UO$_2^{2+}$ concentration vs. illumination time (A) and pseudo-first-order rate constant (k) of UO$_2^{2+}$ reduction (B) over photocatalysts.
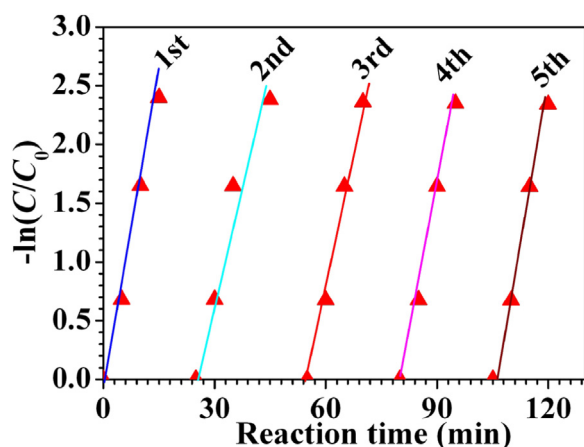
Fig. 8. Cycling runs of SC_3N_4-3 for the photocatalytic reduction of UO_2^{2+}.

Moreover, the activity of the optimal photocatalyst SC_3N_4-3 was compared with the reported photoreductive catalysts (Fig. 7). It is seen that SC_3N_4-3 showed the best activity among the photoreductive catalysts (e.g., P-C_3N_4 [56], $SnIn_4S_8$ [57], CdS-graphene [58], $Bi_{24}O_{31}Br_{10}$ [59], and B-N-F co-doped TiO_2 [60]) in the photoreduction reaction of UO_2^{2+} (Fig. 7A), and k value over SC_3N_4-3 was 1.6, 3.81, 5.16, 6.95, and 10 times of that for P-C_3N_4 (0.10 min^{-1}), $SnIn_4S_8$ (0.042 min^{-1}), $Bi_{24}O_{31}Br_{10}$ (0.031 min^{-1}), CdS-graphene (0.023 min^{-1}) and B-N-F co-doped TiO_2 (0.016 min^{-1}), respectively (Fig. 7B). Besides the good activity, SC_3N_4 exhibited excellent stability in the photoreductive reaction of UO_2^{2+} (Fig. 8). After each reaction, the photocatalyst was collected and treated for the next cycle of photocatalysis test. In the stability test, the photocatalytic activity of SC_3N_4-3 showed no obvious decline during five cycles, and the rate constant of UO_2^{2+} removal reaction over SC_3N_4-3 was kept at around 0.16 min^{-1}. IR characterization presents that SC_3N_4-3 shows good structural stability in the recycle tests (Fig. S3 in Supplementary material). These results indicate that SC_3N_4 with a low cost but high activity shows great potency for photoreduction elimination of UO_2^{2+}.

As described above, unique electronic structure for the so-prepared SC_3N_4 causes excellent photoreduction reactivity. To understand the promoting effect of the graphene-like structure on the photocatalytic activity of SC_3N_4, we investigated the steady and time-resolved fluorescence emission spectra of SC_3N_4 (Fig. 9). The SC_3N_4 samples give a similar band-to-band fluorescence emission feature of C_3N_4 (Fig. 9A). The weak emission signal, nevertheless, reveals the declined radiative recombination ratio of photogenerated electron-hole in the SC_3N_4 samples [32,61–63]. Lifetime for photogenerated electron was further probed with

time-resolved fluorescence spectra (Fig. 9B). Fitting spectrum for fluorescence decay suggests two lifetimes shown in Table 1. The fluorescence lifetime (τ) for C_3N_4 was 1.56 ns, while for the SC_3N_4 samples, the fluorescence lifetimes were shortened to 1.49 (SC_3N_4-1), 1.40 (SC_3N_4-2), and 1.23 ns (SC_3N_4-3). The significant shortening of the fluorescence lifetime is attributed to the non-radiation energy transfer over the graphene-like structure of SC_3N_4 [64–67]. Graphene-like structure could promote the non-radiative energy transfer, and the process is competitive with spontaneous radiation, and thus the fluorescence lifetimes decreased due to the graphene-like structure of SC_3N_4. The rates of the non-radiative transfer ‹k_{ent}› listed in Table 1 were calculated according to the equation ‹k_{ent}› = ‹τ_1›$^{-1}$ – ‹τ_2›$^{-1}$, and the τ_1 and τ_2 are the short and long lifetimes, respectively [68]. The rate of the energy transfer of SC_3N_4-3 was 1.27 times as high as that of g-C_3N_4. Moreover, the electron-transfer rate ‹k_{et}› was calculated to be 0.03, 0.07 or 0.17 ns^{-1} corresponding to SC_3N_4-1, SC_3N_4-2 or SC_3N_4-3 by the equation ‹k_{et}› = ‹$\tau(SC_3N_4)$›$^{-1}$ – ‹$\tau(g\text{-}C_3N_4)$›$^{-1}$ [68]. Apparently, the graphene-like structure induced by sulfur doping can promote the energy transfer and electron transfer rates.

3.4. Photocatalytic reduction mechanism of UO_2^{2+} over SC_3N_4

It is known that the effective utilization of photogenerated electron plays an important role for photoreduction reaction of UO_2^{2+}, and the CB position for SC_3N_4 was confirmed to be −1.28 V, which is more lower compared with the reduction potential of $O_2/·O_2^-$ (−0.28 V) and UO_2^{2+}/UO_2 (0.411 V), thus the existence of oxygen and photogenerated hole (h$^+$) would be the disturbance factors. To further understand the photocatalytic reduction process, the reaction atmosphere of UO_2^{2+} was transformed from N_2 to O_2 before illumination. It can be known that, when O_2 was saturated in the photoreduction with methanol as h$^+$ scavenger, the UO_2^{2+} concentration only decreased from 92% (N_2 with methanol) to 65% within 15 min of irradiation with SC_3N_4-3 as photocatalyst (Fig. 10), indicating that the photogenerated electron was mainly reacted with O_2. When the reaction proceeded in the nitrogen atmosphere without the aid of methanol, the UO_2^{2+} concentration decreased to 52%. Based on these data, we can deduce the photocatalytic mechanism of UO_2^{2+} reduction over the SC_3N_4 combined with its CB and VB potentials as well as the band gap energy (Fig. 11). Introducing S into C_3N_4 reduced the band-gap energy by elevating the CB and VB minimum of SC_3N_4, and electrons were excited from the VB top to CB of SC_3N_4 under visible-light illumination. Due to the large surface area for SC_3N_4, UO_2^{2+} ions would easily adsorb on the SC_3N_4, and the photoexcited charge was transferred to UO_2^{2+}. Therefore, UO_2^{2+} was finally photoreduced to UO_2, and h$^+$ of VB was captured with CH_3OH.
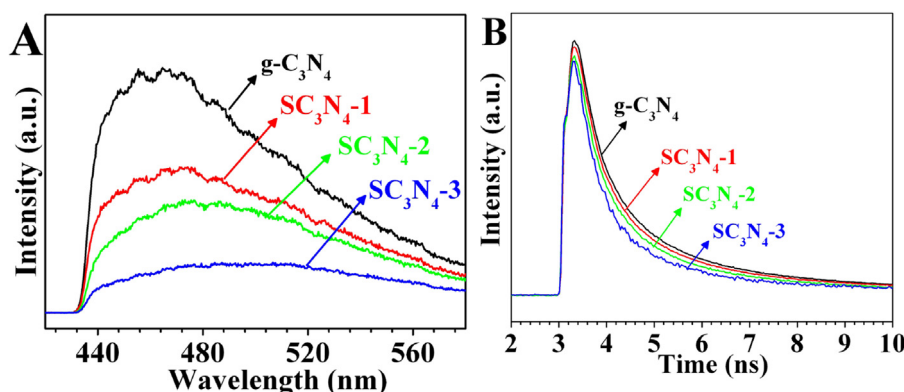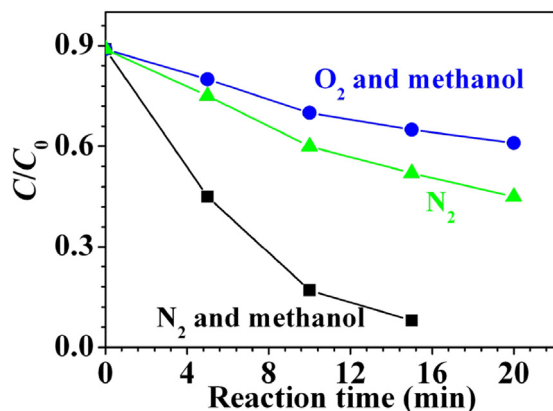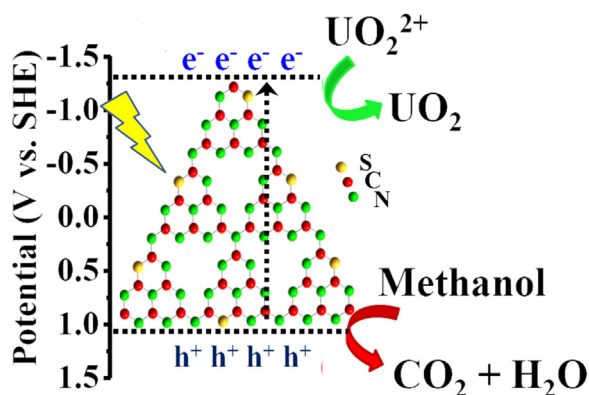

Fig. 9. PL spectra and fluorescence lifetime of g-C_3N_4 and SC_3N_4 samples.

Table 1
Time-resolved fluorescence decay parameters of g-C_3N_4 and SC_3N_4.

Sample	τ_1 (ns)	τ_2 (ns)	τ_{av} (ns)	k_{et} (ns^{-1})	k_{ent} (ns^{-1})
g-C_3N_4	0.89 (85.3%)	5.44 (14.7%)	1.56	–	0.94
SC_3N_4-1	0.85 (86.0%)	5.39 (14.0%)	1.49	0.03	0.99
SC_3N_4-2	0.82 (86.2%)	5.05 (13.8%)	1.40	0.07	1.02
SC_3N_4-3	0.71 (87.4%)	4.82 (12.6%)	1.23	0.17	1.20

Fig. 10. The variation of UO_2^{2+} concentration vs. illumination time over SC_3N_4-3 photocatalyst with N_2, O_2 and/or methanol in the system.

Fig. 11. The photocatalytic reduction reaction and charge transfer mechanism over the SC_3N_4-3 photocatalyst under visible-light irradiation.

4. Conclusions

We designed graphene-like S-doped C_3N_4 (SC_3N_4) photocatalysts for the photoreductive elimination of UO_2^{2+} pollutant. The as-designed C_3N_4 showed high photocatalytic elimination efficiency of UO_2^{2+}, and the photoreactivity of the optimal SC_3N_4 sample was 2.34 times higher than C_3N_4 under visible-light illumination. The remarkable photoactivity of SC_3N_4 is ascribed to the narrowed band gap with an upshifting of CB, VB potentials, and the excellent efficiency of charge transfer and carrier utilization. As revealed by both experimental and theoretical perspectives, these results strongly suggest that construction of graphene-like g-C_3N_4 by doping an element with similar electronegativity to C should be an effective strategy to design efficient visible-light-responsive photocatalysts for energy production and environmental remediation.

Acknowledgments

Appendix A. Supplementary data

Supplementary data associated with this article can be found, in the online version, at http://dx.doi.org/10.1016/j.apcatb.2016.12.043.

References

[1] Q.J. Xiang, J.G. Yu, M. Jaroniec, Chem. Soc. Rev. 41 (2012) 782–796.
[2] H.G. Yu, W.Y. Chen, X.F. Wang, Y. Xu, J.G. Yu, Appl. Catal. B: Environ. 187 (2016) 163–170.
[3] W.T. Ong, L.L. Tan, Y.H. Ng, S.T. Yong, S.P. Chai, Chem. Rev. 116 (2016) 7159–7329.
[4] J.X. Xia, J. Di, H.T. Li, H. Xu, H.M. Li, S.J. Guo, Appl. Catal. B: Environ. 181 (2016) 260–269.
[5] J. Di, J.X. Xia, M.X. Ji, L. Xu, S. Yin, Q. Zhang, Z.G. Chen, H.M. Li, Carbon 98 (2016) 613–623.
[6] S. Chen, P. Slattum, C.Y. Wang, L. Zang, Chem. Rev. 115 (2015) 11967–11998.
[7] H.X. Zhao, S. Chen, X. Quan, H.T. Yu, H.M. Zhao, Appl. Catal. B: Environ. 194 (2016) 134–140.
[8] M.S. Akple, J.X. Low, S. Wageh, A.A. Al-Ghamdi, J.G. Yu, J. Zhang, Appl. Surf. Sci. 358 (2015) 196–203.
[9] Z.J. Ma, R.J. Sa, Q.H. Li, K.C. Wu, Phys. Chem. Chem. Phys. 18 (2016) 1050–1058.
[10] X.P. Xiao, J.H. Wei, Y. Yang, R. Xiong, C.X. Pan, J. Shi, ACS Sustain. Chem. Eng. 4 (2016) 3017–3023.
[11] W.T. Wu, J.Q. Zhang, W.Y. Fan, Z.T. Li, L.Z. Wang, X.M. Li, Y. Wang, R.Q. Wang, J.T. Zheng, M.B. Wu, H.B. Zeng, ACS Catal. 6 (2016) 3365–3371.
[12] X.L. Yang, F.F. Qian, G.J. Zou, M.L. Li, J.R. Lu, Y.M. Li, M.T. Bao, Appl. Catal. B: Environ. 193 (2016) 22–35.
[13] Q. Huang, J.G. Yu, S.W. Cao, C. Cui, B. Cheng, Appl. Surf. Sci. 358 (2015) 350–355.
[14] Q. Han, B. Wang, J. Gao, Z.H. Cheng, Y. Zhao, Z.P. Zhang, L.T. Qu, ACS Nano 10 (2016) 2745–2751.
[15] X.J. She, L. Liu, H.Y. Ji, Z. Mo, Y.P. Li, L.Y. Huang, D.L. Du, H.M. Li, Appl. Catal. B: Environ. 187 (2016) 144–153.
[16] S. Chen, C. Wang, B.R. Bunes, Y.X. Li, C.Y. Wang, L. Zang, Appl. Catal. A: Gen. 498 (2015) 63–68.
[17] S.W. Cao, J.X. Low, J.G. Yu, M. Jaroniec, Adv. Mater. 27 (2015) 2150–2176.
[18] G.H. Dong, L.P. Yang, F. Wang, L. Zang, C.Y. Wang, ACS Catal. 6 (2016) 6511–6519.
[19] G.H. Dong, W.K. Ho, L.Z. Zhang, Appl. Catal. B: Environ. 190 (2016) 26–35.
[20] Y.M. Wu, S. Chen, J. Zhao, X. Yue, W.Y. Deng, Y.X. Li, C.Y. Wang, J. Environ. Chem. Eng. 4 (2016) 797–807.
[21] F. Raziq, Y. Qu, M. Humayun, A. Zada, H.T. Yu, L.Q. Jing, Appl. Catal. B: Environ. 201 (2017) 486–494.
[22] Y.S. Fu, T. Huang, B.Q. Jia, J.W. Zhu, X. Wang, Appl. Catal. B: Environ. 202 (2017) 430–437.
[23] K.N. Ding, L.L. Wen, M.Y. Huang, Y.F. Zhang, Y.P. Lu, Z.F. Chen, Phys. Chem. Chem. Phys. 18 (2016) 19217–19226.
[24] H. Wang, X.D. Zhang, J.F. Xie, J.J. Zhang, P. Ma, B.C. Pan, Y. Xie, Nanoscale 7 (2015) 5152–5156.
[25] S. Lu, C. Li, H.H. Li, Y.F. Zhao, Y.Y. Gong, L.Y. Niu, X.J. Liu, T. Wang, Appl. Surf. Sci. 392 (2017) 966–974.
[26] W.B. Li, C. Feng, S.Y. Dai, J.G. Yue, F.X. Hua, H. Hou, Appl. Catal. B: Environ. 168–169 (2015) 465–471.
[27] J.S. Zhang, J.H. Sun, K. Maeda, K. Domen, P. Liu, M. Antonietti, X.Z. Fu, X.C. Wang, Energy Environ. Sci. 4 (2011) 675–678.
[28] Q.Y. Guo, Y.H. Zhang, J.R. Qiu, G.P. Dong, J. Mater. Chem. C 4 (2016) 6839–6847.
[29] G. Liu, P. Niu, C.H. Sun, S.C. Smith, Z.G. Chen, G.Q. Lu, H.M. Cheng, J. Am. Chem. Soc. 132 (2010) 11642–11648.
[30] K. Wang, Q. Li, B.S. Liu, B. Cheng, W.K. Ho, J.G. Yu, Appl. Catal. B: Environ. 176–177 (2015) 44–52.
[31] C.H. Lu, P. Zhang, S.J. Jiang, X. Wu, S.Q. Song, M.S. Zhu, Z.Z. Lou, Z. Li, F. Liu, Y.H. Liu, Y. Wang, Z.G. Le, Appl. Catal. B: Environ. 200 (2017) 378–385.

[32] C.H. Lu, R.Y. Chen, X. Wu, M.F. Fan, Y.H. Liu, Z.G. Le, S.J. Jiang, S.Q. Song, Appl. Surf. Sci. 360 (2016) 1016–1022.

[33] N. Sagara, S. Kamimura, T. Tsubota, T. Ohno, Appl. Catal. B: Environ. 192 (2016) 193–198.

[34] Z. Li, C. Kong, G.X. Lu, J. Phys. Chem. C 120 (2016) 56–63.

[35] Y.P. Zhu, T.Z. Ren, Z.Y. Yuan, ACS Appl. Mater. Interfaces 7 (2015) 16850–16856.

[36] L.H. Lin, H.H. Qu, Y.F. Zhang, X.C. Wang, ACS Catal. 6 (2016) 3921–3931.

[37] Y.S. Jun, W.H. Hong, M. Antonietti, A. Thomas, Adv. Mater. 21 (2009) 4270–4274.

[38] A. Thomas, A. Fischer, F. Goettmann, M. Antonietti, J.O. Muller, R. Schlogl, J.M. Carlsson, J. Mater. Chem. 18 (2008) 4893–4908.

[39] P. Niu, L.L. Zhang, G. Liu, H.M. Cheng, Adv. Funct. Mater. 22 (2012) 4763–4770.

[40] S.B. Yang, Y.J. Gong, L. Zhang, L.L. Ma, R. Fang, X.C. Wang, P.M. Ajayan, Adv. Mater. 25 (2013) 2452–2456.

[41] X.J. She, H. Xu, Y.G. Xu, J. Yan, J.X. Xia, L. Xu, Y.H. Song, Y. Jiang, Q. Zhang, H.M. Li, J. Mater. Chem. A 2 (2014) 2563–2570.

[42] J.X. Xiang, M.X. Ji, J. Di, B. Wang, S. Yin, Q. Zhang, M.Q. He, H.M. Li, Appl. Catal. B: Environ. 191 (2016) 235–245.

[43] L.H.S. Veiga, E.C.S. Amaral, H.M. Fernandes, J. Environ. Radioact. 39 (1998) 69–85.

[44] R. Busquim e Silva, M.S. Kazimi, P. Hejzlar, Energy Environ. Sci. 3 (2010) 996–1010.

[45] D.L. Clark, D.E. Hobart, M.P. Neu, Chem. Rev. 95 (1995) 25–48.

[46] G. Choppin, J. Radioanal. Nucl. Chem. 273 (2007) 695–703.

[47] Y.H. Wang, M. Frutschi, E. Suvorova, V. Phrommavanh, M. Descostes, A.A.A. Osman, G. Geipel, R. Bernier-Latmani, Nat. Commun. 4 (2013), 2942–2930.

[48] S. Tripathi, R. Bose, A. Roy, S. Nair, N. Ravishankar, ACS Appl. Mater. Interfaces (2015) 26430–26436.

[49] D.D. Shao, Z.Q. Jiang, X.K. Wang, J.X. Li, Y.D. Meng, J. Phys. Chem. B 113 (2009) 860–864.

[50] Y.B. Sun, S.B. Yang, Y. Chen, C.C. Ding, W.C. Cheng, X.K. Wang, Environ. Sci. Technol. 49 (2015) 4255–4262.

[51] F. Bonaccorso, Z. Sun, T. Hasan, A.C. Ferrai, Nat. Photon. 4 (2010) 611–622.

[52] G.H. Dong, W.K. Ho, C.Y. Wang, J. Mater. Chem. A 3 (2015) 23435–23441.

[53] Z. Yang, Z. Yao, G.F. Li, G.Y. Fang, H.G. Nie, Z. Liu, X.M. Zhou, X.A. Chen, S.M. Huang, ACS Nano 6 (2012) 205–211.

[54] V.N. Salomore, J.M. Meichtry, G. Zampieri, M.I. Litter, Chem. Eng. J. 261 (2015) 27–35.

[55] V. Eliet, G. Bidoglio, Environ. Sci. Technol. 32 (1998) 3155–3161.

[56] Y.C. Deng, L. Tang, G.M. Zeng, Z.J. Zhu, M. Yan, Y.Y. Zhou, J.J. Wang, Y.N. Liu, J.J. Wang, Appl. Catal. B: Environ. 203 (2017) 343–354.

[57] L. Wang, X.Y. Li, W. Teng, Q.D. Zhao, Y. Shi, R.L. Yue, Y.F. Chen, J. Hazard. Mater. 244–245 (2013) 681–688.

[58] X.J. Liu, L.K. Pan, T. Lv, G. Zhu, Z. Sun, C.Q. Sun, Chem. Commun. 47 (2011) 11984–11986.

[59] J. Shang, W.C. Hao, X.J. Lv, T.M. Wang, X.L. Wang, Y. Du, S.X. Dou, T.F. Xie, D.J. Wang, J.O. Wang, ACS Catal. 4 (2014) 954–961.

[60] A.E. Giannakas, M. Antonopoulou, C. Daikopoulos, Y. Deligiannakis, I. Konstantinou, Appl. Catal. B: Environ. 184 (2016) 44–54.

[61] J. Di, J.X. Xia, Y. Huang, M.X. Ji, W.M. Fan, Z.G. Chen, H.M. Li, Chem. Eng. J. 302 (2016) 334–343.

[62] J. Di, J.X. Xia, M.X. Ji, B. Wang, S. Yin, Y. Huang, Z.G. Chen, H.M. Li, Appl. Catal. B: Environ. 188 (2016) 376–387.

[63] J. Di, J.X. Xia, M.X. Ji, B. Wang, X.W. Li, Q. Zhang, Z.G. Chen, H.M. Li, ACS Sustain. Chem. Eng. 4 (2016) 136–146.

[64] D. Kozawa, X. Zhu, Y.H. Miyauchi, S. Mouri, M. Ichida, H.B. Su, K. Matsuda, J. Phys. Chem. Lett. 5 (2014) 1754–1759.

[65] L. Gaudreau, K.J. Tielruoij, G.E.D.K. Prawiroatmodjo, J. Qsmond, F.J. Garcia de Abajo, Nano Lett. 13 (2013) 2030–2035.

[66] R. Maiti, S. Mukherjee, S. Haldar, D. Bhowmick, S.K. Ray, Carbon 104 (2016) 226–232.

[67] H.S.S.R. Matte, K.S. Subrahmanyam, K.V. Rao, S.J. George, Chem. Phys. Lett. 506 (2011) 260–264.

[68] M.S. Zhu, Y.P. Dong, Y.K. Du, Z.G. Mou, J. Liu, P. Yang, X.M. Wang, Chem. Eur. J. 18 (2012) 4367–4374.